Configuration Modeling of a Soft Robotic Element with Selectable Bending Axes*

Emily A. Allen¹, Brandon C. Townsend¹ and John P. Swensen¹

Abstract—This paper presents an approach for modeling new soft robotic materials which possess the ability to control directional stiffness. These materials are inspired by biological systems where movements are enabled by variable stiffness tissue and contraction of localized muscle groups. Here a lowmelting-point (LMP) material lattice embedded in an elastomer serves as a rigid skeleton that may be locally melted to allow bending at selectable joint locations. The forward kinematics of the lattice has been modeled using the product of exponentials method with the incorporation of bending axis selectivity. In this paper, we develop this model to account for torques imposed by tendons, and we model the elastomer's resistance to bending as a torsional spring at the selected joints. Thus we obtain a twoway relationship between tendon forces and joint angles/axes. The concept of applying traditional robot modeling strategies to selectively compliant robotic structures could enable precise control of dexterous soft robots that satisfy stringent safety criteria.

I. INTRODUCTION

Several novel approaches to soft robotics actuation have been innovated in the last several years as researchers explore the soft robotics alternative to traditional rigid robots. With the growing demand for at-home healthcare and the push for industrial co-robots, safety and adaptability are a high priority for modern robots [1]. The intrinsically soft nature of the soft robotics approach offers solutions to safety concerns and shows great promise for mimicking human abilities [2]–[4]. Unlike traditional robots, soft robots can deform upon impact to prevent injuries. Several approaches have been developed to address the strength/flexibility trade-off introduced by the soft robotics approach [1], [5].

In an effort to maintain the structural integrity of traditional robots, variable stiffness actuators operate by varying the stiffness transmitted to joints between rigid links. Antagonistic arrangements of actuators mimic human muscle configuration and can exhibit a nonlinear relationship between input torque and angular joint deflection [6]–[8]. Other methods use advanced control systems to enable variable stiffness. Although these methods offer high-level precision and reliability, their practicality is limited by size, weight and bandwidth, and they are generally not suitable for material actuators with multiple degrees of freedom [9], [10].

Variable stiffness structures are comprised of prestressed struts and cables that hold the structure in a configuration; by selectively releasing and re-tensioning cables within a robotic system, a variety of predictable motions may be activated [11]–[13]. Similarly, the application of 4D printing to soft robotics has enabled assemblies that self-bend when exposed to light, heat, electricity, or other means of stimulation. A patterned deposition of ink causes heating/shrinkage at folding sites or localized swelling of media within polymer matrices under infrared exposure [14], [15]. Other researchers have designed robotic structures using origami techniques [16], [17]. Soft robotic actuators for specific applications are often designed to meet the compliance requirements of the system at hand [18]. Many soft actuators are fabricated with geometrically patterned pneumatic chambers that deform the elastomer when pressurized [19]–[23]. Although elastomers are inherently weak, fiber reinforcement and high pressure supplies offer surprisingly high strength capabilities [4], [24], [25].

Research similar to the work in this paper is driven by a need for soft robotic structures/materials that can exhibit both high strength and compliant behavior. The impressive capabilities of biological systems such as muscular hydrostats and catch-connective tissue inspire the design of soft robotic materials whose stiffness can be precisely controlled [26], [27]. Some researchers have explored the use of low-melting-point (LMP) materials to enable stiffness variability [28]–[33]. Heating of these materials causes the internal skeleton to melt and allow compliant behavior when desired.

These concepts are expanded to enable directional stiffness control by locally melting the skeleton at designated locations [34]. In this work, we propose a method for modeling the configuration such an element with selectable bending axes.

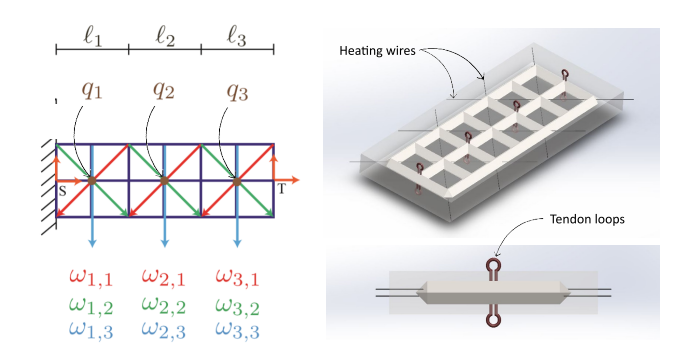


Fig. 1. Design of 3-link soft robotic element with internal LMP lattice that can be selectively melted to allow bending about 9 different axes.

^{*}This research was funded by the National Science Foundations National Robotics Initiative Award 1734117

¹Emily Allen, Brandon Townsend and John Swensen are with the School of Mechanical and Materials Engineering, Washington State University, Pullman, WA 99164 emily.allen2@wsu.edu, brandon.townsend@wsu.edu, john.swensen@wsu.edu



Fig. 2. A few unique configurations achievable through selective melting and deformation of soft robotic element.

A 3-link soft robotic element has been proposed with an internal rigid skeleton that may be selectively melted to allow bending about specified axes as shown in Fig. 1. The element consists of a low-melting-point (LMP) metal or polymer lattice encased in silicone rubber with nichrome heating elements arranged to allow selection of bending axes.

The nine selectable bending axes represented by $\omega_{i,j}$, are shown in Fig. 1, where i refers to the segment number and j is the axis direction. For this problem, up to 3 of the 9 bending axes may be selected at once (up to one axis per segment) by localized melting of the lattice. As shown in Fig. 3, a tendon is attached to each side of the element to induce bending about the selected compliant axes. The forward kinematics of this element have been constructed using the product of exponentials method to determine the configuration of the piece based on the selected axes and corresponding joint angles [34]. A variety of unique configurations may be achieved as shown in Fig. 2 with minimal complexity.

For this paper, we take this model a step further by relating the forces applied on tendons to the deformation of the piece. This involves modeling the joints (melted axes) as torsional springs with some constant stiffness. By relating the tendon forces and the elements configuration, we may determine what configurations are possible for any given set of selected axes.

Each set of equations is derived as a function of ω , the set of selected axes which may include a single axis or up to 3 of the 9 possible bending axes (one axis per segment). Each time that a segment is deformed and then cooled, the reference configuration of the model changes and must be updated. By successively melting different joints and controlling tendon forces, a vast range of configurations may be achieved by this simple element.

Selective melting drastically improves the work space of the device as compared to simultaneous melting by allowing for finer control using only a single tendon. When individual joints may be selected to melt on their own, or even in pairs rather than all three, then the shape of the device may be more precisely controlled.

Simultaneous melting only allows for the bending of all selected joints at once, with each joint experiencing approximately the same angular displacement. This provides both little control and limited workspace. Selective melting

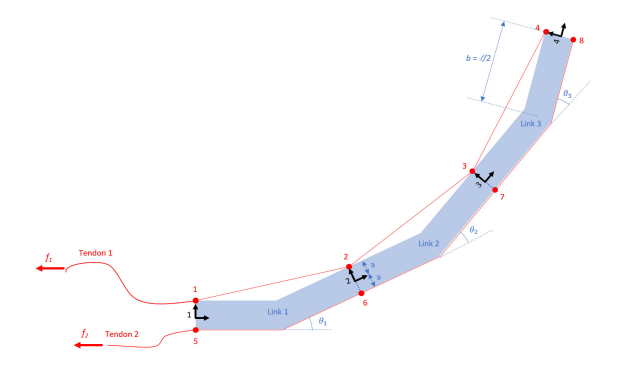


Fig. 3. Tendon routing diagram for 3-link soft robotic element.

allows for configurations and tool tip positions that would not otherwise be achievable by allowing for the manipulation of individual joints while the other joints are fixed.

II. MATERIALS AND METHODS

A. Extension Functions for Tendons

The torque applied on the joints by the tendons depends on the tendon routing configuration and the axes that have been selected. For example, if the tendon does not lie perpendicular to the selected bending axis, a larger tendon force will be required to achieve the same torque about the joint. These geometric relationships between tendon force and joint torque are derived as a function of each possible axis selection, joint angle, and tendon offset.

The joint torques τ may be directly related to the forces applied to the tendons by developing extension functions for each tendon. This method of analyzing inelastic tendons is described by Murray et al. [35]. This method involves deriving the extension function for each tendon, which expresses the length of the tendon as a function of the joint angles. In our case, since the axis directions may vary, the extension functions are a function of both the joint angles and the selected axes.

For a simple planar problem, developing these extension functions may be done by simply analyzing the geometry. For example, if the axes $\omega_{1,3}, \omega_{2,3}$, and $\omega_{3,3}$, are selected, the geometric relationships may be extracted by inspection of Fig. 3. However, when different axes are selected, the problem is no longer planar, and these geometric relations become nontrivial.

Rather than developing complicated, three-dimensional geometric relationships for each bending axis combination, the forward kinematics exponential may be used to express the length of each tendon for any set of selected axes and joint angles. The length of tendon 1, as shown in Fig. 3, is simply the sum of the distances between tendon fixation points 1 and 2, 2 and 3, 3 and 4. These distances are already known from the forward kinematics for this element, which have been previously developed [34]

$$x_{1,1}(\theta_1, \omega_1) = \begin{bmatrix} 0\\0\\a\\1 \end{bmatrix}, \tag{1}$$

$$x_{2,1}(\theta_1, \omega_1) = e^{\widehat{\xi_1(\omega_1)}\theta_1} g_{1,2_0} \begin{bmatrix} 0\\0\\a\\1 \end{bmatrix},$$
 (2)

where $\xi_1(\omega_1)$ is the twist used to represent the rotation and translation of points due to bending about the selected axis ω_1 . Here the second subscript indicates the frame of reference, so $x_{2,1}$ represents the homogeneous coordinates of point 2 relative to frame 1. The matrix exponential $e^{\hat{\xi}_1\theta_1}$ used to transform points from frame 1 to 2 has been previously developed as a function of ω in the construction of the forward kinematics relationships for this element [34]. The reference configuration $g_{1,2_0}$ is the transformation between frames 1 and 2 when $\theta_1=0$. For this case,

$$g_{1,2_0} = \begin{bmatrix} 1 & 0 & 0 & \ell_1 \\ 0 & 1 & 0 & 0 \\ 0 & 0 & 1 & 0 \\ 0 & 0 & 0 & 1 \end{bmatrix}, \tag{3}$$

where ℓ_1 is the length of link 1. The distance between $x_{1,1}$ and $x_{2,1}$ may then be computed as:

$$d_{1-2}(\theta_1, \omega_1) = \sqrt{(x_{1,1}^\top x_{1,1})^2 + (x_{2,1}^\top x_{2,1})^2}.$$
 (4)

Finally, when the joint angles are all positive, the extension function for tendon 1 may then be computed by summing the distances between each tendon fixation point:

$$h_1(\theta,\omega) = d_{1-2} + d_{2-3} + d_{3-4},\tag{5}$$

where d_{2-3} and d_{3-4} are computed using the matrix exponential for rotation about ω_2 and ω_3 . The extension function for tendon 2 may simply be expressed as

$$h_2(\theta,\omega) = \ell_1 + a\theta_1 + \ell_2 + a\theta_2 + \ell_3 + a\theta_3$$
 (6)

when the joint angles are all positive. In theory, there are 8 different cases for these extension functions based on different combinations of positive and negative joint angles. For example, if θ_1 and θ_2 are positive while θ_3 is negative, the extension functions would behave differently than if all the joint angles were positive. Thus, extension functions are different for each of the 8 cases of positive/negative joint angle combinations. However, for this project we only have two tendons, so if we consider only simultaneous melting, the only possible joint angle combinations are case 1 (all joint angles are positive) and case 8 (all joint angles are negative). For case 8, the joint angles are all negative (i.e. tendon 2 is activated instead of tendon 1), and the extension functions are reversed as follows:

$$h_1(\theta, \omega) = \ell_1 - a\theta_1 + \ell_2 - a\theta_2 + \ell_3 - a\theta_3,$$
 (7)

$$h_2(\theta,\omega) = d_{5-6} + d_{6-7} + d_{7-8}. (8)$$

B. Coupling Matrix

According to Murray et al. [35], by applying the conservation of energy, the joint torques can be expressed as

$$\tau = P(\theta, \omega)f,\tag{9}$$

where f is a vector containing the forces on each tendon:

$$f = \begin{bmatrix} f_1 \\ f_2 \end{bmatrix}, \tag{10}$$

and where $P(\theta, \omega)$ is the coupling matrix computed from

$$P(\theta, \omega) = \frac{\partial h^{\top}(\theta, \omega)}{\partial \theta}, \tag{11}$$

where h is a vector containing the extension functions for the appropriate case of positive/negative joint angle combinations:

$$h(\theta, \omega) = \begin{bmatrix} h_1(\theta, \omega) \\ h_2(\theta, \omega) \end{bmatrix}. \tag{12}$$

The computation of $P(\theta,\omega)$ is non-trivial. Since the extension functions h depend on the joint angles and selected axes, and they involve matrix exponentials and square roots, taking the derivatives for $P(\theta,\omega)$ by hand would be tedious and nearly impossible. The extension functions were entered into Mathematica for the analytical computation of these derivatives. These derivatives were computed for all 8 cases of positive/negative joint angle combinations. The resulting coupling matrix for each case, expressed as a function of $\theta,\omega,a,\ell_1,\ell_2,$ and $\ell_3,$ was then converted to MATLAB using the ToMatlab package.

C. Measuring Joint Stiffnesses

The joint stiffness modeled by the torsional springs is dependent on the geometry of the element at the joint and the material properties of the elastomer. By assuming Hooke's Law behavior, the torque exerted by the spring (joint) can be expressed as

$$\tau = k\theta,\tag{13}$$

where θ is the resulting joint angle relative to the equilibrium configuration, and k is the spring constant which may be determined experimentally. The spring constant k should be proportional to the elastic modulus of the material and the area moment of inertia of the joint cross-section. k may be determined experimentally for a simple geometry and then scaled to find k for other joint geometries (with different area moments of inertia).

For this particular project, there are only two different cross-sections for the nine different allowable bending axes. There is a cross-section for the straight (transverse) axes, and a slightly wider cross-section for the diagonal axes. A primitive experiment setup shown in Fig. 4 was used to measure the effective spring constants of these melted joints

on the soft robotic element. The desired axis was heated to $60\,^{\circ}\mathrm{C}$ to melt the polycaprolactone (PCL) polymer lattice along the axis, then the tendon was pulled with a load cell to measure the perpendicular force required to incur a $90\,^{\circ}$ bend at the axis; average force measurements from 3 identical repeated tests were then converted to torsional spring constants listed in the table below.



Fig. 4. Experimental testing of effective torsional spring constants representing resistance to deformation at selectively melted joints.

TABLE I

MEASURED TORSIONAL SPRING CONSTANTS FOR STRAIGHT AND

DIAGONAL AXES

Axis Type	Measured Spring Constant	Variable Name
Straight (melted)	21.7 ± 1.4 N·mm/rad	$k_{straight}$
Diagonal (melted)	27.0 ± 1.0 N·mm/rad	$k_{diagonal}$
Straight (solid)	115 ± 11 N⋅mm/rad	k_{solid}

The appropriate stiffness value ($k_{\text{straight}}, k_{\text{diagonal}}$, or k_{solid}) is selected in MATLAB based on the input axis selections using if statements. For example, using the conventions we have chosen, k_i represents the joint stiffness for segment i of the robotic element. If the input ω_i is 1 or 2, this indicates bending about the axis $\omega_{i,1}$ or $\omega_{i,2}$ which are diagonal axes, so k_i is set to be $k_{diagonal}$. If ω_i is 3, this indicates bending about $\omega_{i,3}$, the transverse axis, so k_i is set to be $k_{straight}$. Finally, if ω_i is 0, this indicates an unmelted joint, so k_i is set to be k_{solid} .

The bending resistance at the joints will appear in the potential energy terms in the derivation of the system dynamics using the Lagrange-Euler method.

D. Euler-Lagrange Method to Relate Potential Energy to Joint Torques

The Euler-Lagrange method may be used to develop the equations of motion for the robotic element. Since we are only dealing with the statics of this problem, the higher order terms in this method may be neglected. In other words, we can neglect the effects of kinetic energy and rotational inertia on the system. We will also choose to neglect gravity for this paper. By simplifying the problem in this way, the resulting governing equation will take the form:

$$\frac{-\partial \mathcal{L}(\theta, \omega)}{\partial \theta} = K(\omega)\theta = \tau^{\top}, \tag{14}$$

where $\mathcal{L}(\theta,\omega)$ is the Lagrangian, θ is the joint angles, and τ is the joint torques vector.

Beginning with the equation for the potential energy of the system, we account for the torques generated by the bending at the joints:

$$PE = \frac{1}{2}k_1\theta_1^2 + \frac{1}{2}k_2\theta_2^2 + \frac{1}{2}k_3\theta_3^2, \tag{15}$$

with k_i being the stiffness of the joint and θ_i being the angular displacement at that joint. Given that only potential energy is being considered in the system, the Lagrangian is simply

$$\mathcal{L} = \frac{1}{2}(-k_1\theta_1^2 - k_2\theta_2^2 - k_3\theta_3^2). \tag{16}$$

Differentiating the Lagrangian with respect to θ yields

$$\frac{\partial \mathcal{L}}{\partial \theta} = \begin{bmatrix} -k_1 \theta_1 & -k_2 \theta_2 & -k_3 \theta_3 \end{bmatrix}. \tag{17}$$

Applying the Euler-Lagrange equation to the simplified static model yields the following relationship

$$\tau^{\top} = -\frac{\partial \mathcal{L}}{\partial \theta} = \begin{bmatrix} k_1 \theta_1 & k_2 \theta_2 & k_3 \theta_3 \end{bmatrix}.$$
 (18)

By applying the relationship from (9), the joint torques may be expressed in terms of the tendon forces and coupling matrix. Combining (9) and (22) produces the relationship

$$K(\omega)\theta = P(\theta, \omega)f,$$
 (19)

where $K(\omega)$ is the joint stiffness matrix:

$$K(\omega) = \begin{bmatrix} k_1(\omega) & 0 & 0\\ 0 & k_2(\omega) & 0\\ 0 & 0 & k_3(\omega) \end{bmatrix}.$$
 (20)

In our system, we want to be able to determine θ given a particular f and ω . We also hope to be able to determine f for a given θ and ω . To determine θ from a given f and ω , we can left-multiply each side of (19) by the inverse of the stiffness matrix to yield

$$\theta = \begin{bmatrix} \theta_1 \\ \theta_2 \\ \theta_3 \end{bmatrix} = K^{-1}(\omega)P(\theta, \omega)f. \tag{21}$$

The joint angles θ cannot be solved for analytically in this expression since the coupling matrix P is a complicated function of θ . Since θ appears on both sides of (21), numerical analysis must be applied. This equation can easily be solved using fixed point iteration to determine the joint angles that result from a given set of selected axes ω and tendon forces f. To find the forces required to produce a desired set of joint angles, we simply left multiply (19) by P-inverse to obtain:

$$f = \begin{bmatrix} f_1 \\ f_2 \end{bmatrix} = P^{-1}(\theta, \omega) K(\omega) \theta. \tag{22}$$

III. RESULTS AND DISCUSSION

A. Configuration Computation

By activating different heating elements and applying different tendon forces, a wide variety of configurations may be achieved. A relationship has been developed that enables computation of the joint angles that result from application of a given tendon force. For example, Fig. 5 (a) shows the computed equilibrium configuration when a 4-Newton force is applied to the upper tendon, and the heating elements are activated to allow bending along axes $\omega_{1,1}$ (diagonal axis on first link) and $\omega_{3,3}$ (transverse axis on third link). Other unique configurations may be achieved by applying different tendon forces and selectively melting different axes along the lattice, as seen in Fig. 5 (b) and (c).

Various configurations may be used to perform intelligent tasks. For example, applying a 14-Newton force to the upper tendon while melting parallel diagonal axes could allow the robot to grab a pen as shown below in Fig. 6.

B. Workspace Limitations

It is interesting to note that (21) fails to compute realistic joint angles if a joint angle exceeds 90° along a diagonal axis. At first glance, this may appear to be a computational error, but in reality, this computational limitation perfectly represents a physical limitation. Careful inspection of the tendon routing shown in Figs. 1 and 3 reveals the reason for this limitation. For this particular arrangement of tendon fixation points, the tendon length across a diagonal joint reaches a minimum when the joint angle is 90°. Bending a diagonal joint beyond 90° would actually require elongation of the tendon, so the physical model would never actually bend more than 90° along a diagonal axis. However, along the transverse axes, the physical element can bend beyond 90°, up to the point of folding on itself. This concept is again modeled perfectly by the mathematical model, which allows bending beyond 90° along transverse axes.

C. Force Computation

The ability to compute the tendon forces required to achieve a configuration is desirable for implementing advanced control and maneuverability with the soft robotic element. The relationship from (22) enables this computation. For example, the configuration shown in Fig. 5 (a) was achieved by applying a 4-Newton force to the upper tendon while melting axes $\omega_{1,1}$ and $\omega_{3,3}$. Applying (21) revealed that this load/axis combination results in joint angles of 21.7° , 6.0° , and 93.9° , respectively. We can then test the validity of the force computation function by solving this problem backwards and comparing the force results with the original input force values. To do this, we use 21.7°, 6.0°, and 93.9° as the θ input in (22), along with the axis selection $\omega_{1,1}$ and $\omega_{3,3}$ to determine the forces needed to achieve these joint angles. The forces computed should theoretically be 4 Newtons on the upper tendon and 0 Newtons on the lower tendon. Application of (22) with these input values indicated that forces of 3.9992 N and -0.0009 N on the upper and lower tendons are required to achieve the particular

configuration shown in Fig. 5 (a). These results are not perfect, but they show that (22) is useful for calculating the tendon forces required to achieve a desired set of joint angles with reasonable accuracy.

D. Joint Space Limitations

It is important to note that in the case of this 3-segment element with 2 opposing tendons, not all joint angle combinations are possible. The joint space is limited, and the required force computation only works when the desired joint angles lie within the allowable joint space. This detail is evidenced by both the physical model and the mathematics behind the force computation. From the physical model, we can intuitively see that the angles of the 3 simultaneouslymelted joints cannot be controlled independently with the use of only one tendon. Here we consider only one tendon since it would be counter-productive to pull both tendons simultaneously. Increasing the tendon tension increases the joint angles of all three joints simultaneously in a specific ratio that is proportional to the relative bending stiffnesses of the three joints. In order to compute the tendon force required to achieve a desired set of joint angles, these joint angles must follow the proper ratio proportional to their bending stiffnesses. Otherwise, no tendon force will be able to cause joint angles that do not follow this ratio. For example, no tendon force will be able to cause bending in only the first joint if three joints are melted. Mathematically, this concept is demonstrated in the form of the coupling matrix P. Computing the required tendon forces involves multiplying by the inverse of P, as seen in (22). Recall that P is a 3×2 matrix in this case. As such, the force computation only works when

$$\theta \in Image[K^{-1}(\omega)P(\theta,\omega)].$$
 (22)

However, the restriction on θ for the force computation is actually even more stringent due to the tendon antagonism. Since one of the tendon forces is always zero, θ must be a scalar multiple of a single column of $[K^{-1}(\omega)P(\theta,\omega)]$ for computation of the tendon forces to be possible.

E. Effects of Successive Melting

By successively melting joints, a larger number of more complex configurations are made possible. Notably, it allows for the combination of movements which require both the top and bottom tendons to be pulled. As seen in Fig. 7 (a) and (b), a single joint was melted to achieve a position by pulling the top and bottom tendons, respectively. With successive melting, these configurations can be combined to achieve the configuration shown in in Fig. 7 (c). This combined configuration is not achievable with simultaneous melting, as both the top and bottom tendons must be pulled to achieve the final form. If both axes were melted simultaneously and each tendon pulled, the joints would not be able to bend in opposite directions like they can when sequentially melted.

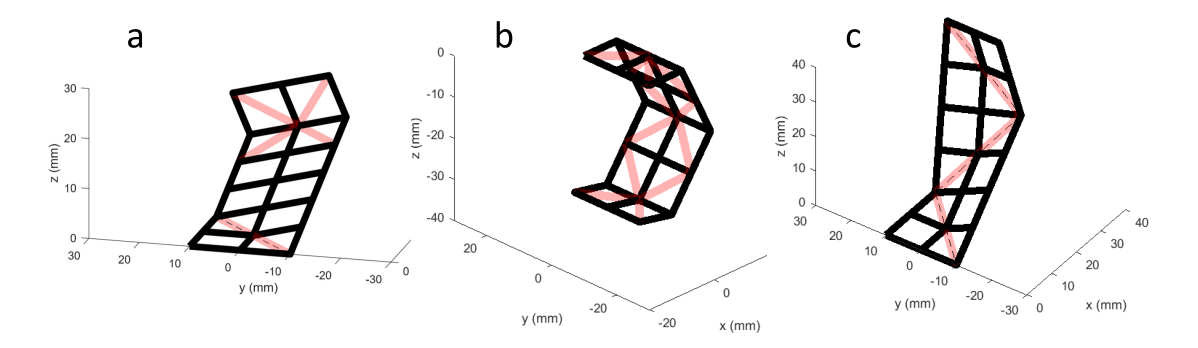


Fig. 5. Simulated configurations of 3-link element under different heating and tendon loads, where red lines indicate activated heating elements.



Fig. 6. Melting parallel diagonal axes allows physical element to wrap around a pen.

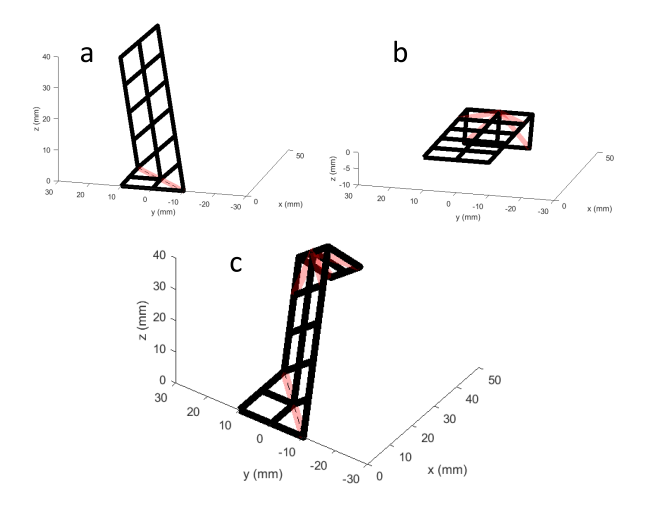


Fig. 7. Example of 2-directional bending enabled by successive melting. (a) and (b) show individual steps; (c) shows resulting configuration from successive deformation.

IV. CONCLUSION

Ultimately, a relationship has been obtained to relate tendon forces to resulting joint angles in the static equilibrium of a 3-segment soft robotic element with selectable axes. With some limitations, this relationship can be used both ways: to compute joint angles given tendon forces and selected axes, or to compute necessary tendon forces to achieve a desired set of joint angles for a given set of selected axes. Using (21) and (22), the joint angles are related to the tendon forces required to produce a desired position using the coupling matrix. The derivation of the application of the coupling matrix is detailed in chapter 4 section 4.1 of A Mathematical Introduction to Robotic Manipulation [35]. The joint stiffnesses were modeled as torsional springs with spring constants that were measured experimentally by melting a joint and pulling a perpendicular tendon using a force meter.

The next step for this project would be to incorporate the dynamics of the system. For this static model, we have neglected the kinetic energy and rotational inertia components. Including these elements in the model will allow us to implement torque control in the future so that we may accurately control the movement of the element and achieve desired trajectories. In the future, it may be helpful to develop an intelligent method of determining which axes need to be melted in order to achieve a desired trajectory. This may be done by determining which set of axes make the desired trajectory lie within the image of the spatial manipulator jacobian. However, for this work the selected axes are a simple input.

Once these relationships are developed, they may then be applied to larger scale robotic elements that include more segments or even three-dimensional structures. We have seen in this project the unique configurations enabled by the selective melting of a small soft robotic element. With just one set of tendons and 3 joints, a wide variety of movements and configurations may be achieved, as evidenced by the ability to grasp a pencil, curl into a tight ball or extend out as a rigid arm. By applying these concepts into higher dimensional structures, highly dexterous movements even mimicking human gestures may be achieved.

ACKNOWLEDGMENT

Special thanks to Lee Taylor for assistance with 3D printing of the PCL polymer lattice for the test piece.

REFERENCES

[1] S. Kim, C. Laschi, and B. Trimmer, "Soft robotics: a bioinspired evolution in robotics," *Trends in Biotechnology*, vol. 31, no. 5, pp. 287 – 294, 2013. [Online]. Available: http://www.sciencedirect.com/science/article/pii/S0167779913000632

- [2] C. Laschi, B. Mazzolai, and M. Cianchetti, "Soft robotics: Technologies and systems pushing the boundaries of robot abilities," *Science Robotics*, vol. 1, no. 1, 2016.
- [3] C. Majidi, "Soft robotics: A perspective current trends and prospects for the future," *Soft Robotics*, vol. 1, no. 1, pp. 5–11, 2014. [Online]. Available: https://doi.org/10.1089/soro.2013.0001
- [4] H. K. Yap, H. Yong Ng, and R. C.-H. Yeow, "High-force soft printable pneumatics for soft robotic applications," *Soft Robotics*, vol. 3, pp. 144–158, 09 2016.
- [5] G.-Z. Yang, J. Bellingham, P. E. Dupont, P. Fischer, L. Floridi, R. Full, N. Jacobstein, V. Kumar, M. McNutt, R. Merrifield, B. J. Nelson, B. Scassellati, M. Taddeo, R. Taylor, M. Veloso, Z. L. Wang, and R. Wood, "The grand challenges of science robotics," vol. 3, no. 14, 2018. [Online]. Available: http://robotics.sciencemag.org/content/3/14/eaar7650
- [6] G. Tonietti, R. Schiavi, and A. Bicchi, "Design and control of a variable stiffness actuator for safe and fast physical human/robot interaction," in *Robotics and Automation*, 2005. ICRA 2005. Proceedings of the 2005 IEEE International Conference on. IEEE, 2005, pp. 526–531.
- [7] R. Schiavi, G. Grioli, S. Sen, and A. Bicchi, "Vsa-ii: a novel prototype of variable stiffness actuator for safe and performing robots interacting with humans," in *Robotics and Automation*, 2008. ICRA 2008. IEEE International Conference on. IEEE, 2008, pp. 2171–2176.
- [8] N. G. Tsagarakis, I. Sardellitti, and D. G. Caldwell, "A new variable stiffness actuator (compact-vsa): Design and modelling," in *Intelligent Robots and Systems (IROS)*, 2011 IEEE/RSJ International Conference on. IEEE, 2011, pp. 378–383.
- [9] N. L. Tagliamonte, F. Sergi, D. Accoto, G. Carpino, and E. Guglielmelli, "Double actuation architectures for rendering variable impedance in compliant robots: A review," *Mechatronics*, vol. 22, no. 8, pp. 1187–1203, 2012.
- [10] B. Vanderborght, A. Albu-Schäffer, A. Bicchi, E. Burdet, D. G. Caldwell, R. Carloni, M. Catalano, O. Eiberger, W. Friedl, G. Ganesh, et al., "Variable impedance actuators: A review," Robotics and autonomous systems, vol. 61, no. 12, pp. 1601–1614, 2013.
- [11] C. Paul, J. W. Roberts, H. Lipson, and F. V. Cuevas, "Gait production in a tensegrity based robot," in *ICAR'05. Proceedings.*, 12th International Conference on Advanced Robotics, 2005. IEEE, 2005, pp. 216–222.
- [12] M. Shibata, F. Saijyo, and S. Hirai, "Crawling by body deformation of tensegrity structure robots," in *Robotics and Automation*, 2009. ICRA'09. IEEE International Conference on. IEEE, 2009, pp. 4375– 4380
- [13] C. Paul, F. J. Valero-Cuevas, and H. Lipson, "Design and control of tensegrity robots for locomotion," *IEEE Transactions on Robotics*, vol. 22, no. 5, pp. 944–957, 2006.
- [14] A. Zolfagharian, A. Kaynak, S. Y. Khoo, and A. Kouzani, "Pattern-driven 4d printing," Sensors and Actuators A: Physical, vol. 274, pp. 231 – 243, 2018. [Online]. Available: http://www.sciencedirect.com/science/article/pii/S0924424718300621
- [15] J.-W. Su, X. Tao, H. Deng, C. Zhang, S. Jiang, Y. Lin, and J. Lin, "4d printing of a self-morphing polymer driven by a swellable guest medium," *Soft Matter*, vol. 14, pp. 765–772, 2018. [Online]. Available: http://dx.doi.org/10.1039/C7SM01796K
- [16] E. Vander Hoff, D. Jeong, and K. Lee, "Origamibot-i: A thread-actuated origami robot for manipulation and locomotion," in 2014 IEEE/RSJ International Conference on Intelligent Robots and Systems. IEEE, 2014. pp. 1421–1426.
- [17] E. Vander Hoff, D. Jeong, and K. Lee, "Origamibot-i: A thread-actuated origami robot for manipulation and locomotion," in 2014 IEEE/RSJ International Conference on Intelligent Robots and Systems, Sep. 2014, pp. 1421–1426.
- [18] C. Majidi, "Soft robotics: a perspective-current trends and prospects for the future," *Soft Robotics*, vol. 1, no. 1, pp. 5–11, 2014.
- [19] F. Daerden and D. Lefeber, "Pneumatic artificial muscles: actuators for robotics and automation," *European journal of mechanical and environmental engineering*, vol. 47, no. 1, pp. 11–21, 2002.
- [20] D. Trivedi, C. Rahn, W. Kier, and I. Walker, "Soft robotics: Biological inspiration, state of the art, and future research," *IEEE ICRA*, vol. 5, no. 3, pp. 99–117, 2008.
- [21] P. Beyl, M. Van Damme, R. Van Ham, B. Vanderborght, and D. Lefeber, "Pleated pneumatic artificial muscle-based actuator system as a torque source for compliant lower limb exoskeletons," *Mechatronics, IEEE/ASME Transactions on*, vol. 19, no. 3, pp. 1046–1056, 2014.

- [22] A. Miriyev, G. Caires, and H. Lipson, "Functional properties of silicone/ethanol soft-actuator composites," *Materials & Design*, vol. 145, pp. 232 – 242, 2018. [Online]. Available: http://www.sciencedirect.com/science/article/pii/S0264127518301485
- 23] D. Rus and M. Tolley, "Design, fabrication and control of soft robots," Nature, vol. 521, no. 7553, pp. 467–475, 2015.
- [24] P. Polygerinos, Z. Wang, J. T. B. Overvelde, K. C. Galloway, R. J. Wood, K. Bertoldi, and C. J. Walsh, "Modeling of soft fiber-reinforced bending actuators," *IEEE Transactions on Robotics*, vol. 31, no. 3, pp. 778–789, June 2015.
- [25] N. Tan, X. Gu, and H. Ren, "Design, characterization and applications of a novel soft actuator driven by flexible shafts," *Mechanism and Machine Theory*, vol. 122, pp. 197 – 218, 2018. [Online]. Available: http://www.sciencedirect.com/science/article/pii/S0094114X1731087X
- [26] K. Schmidt-Nielsen, Animal physiology: adaptation and environment. Cambridge University Press, 1997.
- [27] W. Kier and K. Smith, "Tongues, tentacles and trunks: the biomechanics of movement in muscular-hydrostats," *Zoological Journal of the Linnean Society*, vol. 83, pp. 307 324, 04 1985.
- [28] E. A. Allen, L. D. Taylor, and J. P. Swensen, "Smart material composites for discrete stiffness materials," in *Proc. ASME 2018 Conference on Smart Materials, Adaptive Structures and Intelligent Systems (SMASIS2018)*, San Antonio, TX, 2018, p. V002T06A015.
- [29] W. Shan, T. Lu, and C. Majidi, "Soft-matter composites with electrically tunable elastic rigidity," *Smart Materials and Structures*, vol. 22, no. 8, p. 085005, 2013.
- [30] W. Wang, H. Rodrigue, and S.-H. Ahn, "Smart soft composite actuator with shape retention capability using embedded fusible alloy structures," *Composites Part B: Engineering*, vol. 78, pp. 507–514, 2015.
- [31] T. Schubert and D. Floreano, "Variable stiffness material based on rigid low-melting-point-alloy microstructures embedded in soft poly(dimethylsiloxane) (pdms)," RSC Advances, vol. 3, pp. 24671– 24679, 2013.
- [32] W. Shan, S. Diller, A. Tutcuoglu, and C. Majidi, "Rigidity-tuning conductive elastomer," *Smart Mater. Struct.*, vol. 24, no. 6, pp. 065– 001, 2015.
- [33] M. McEvoy and N. Correll, "Shape change through programmable stiffness," vol. 109, pp. 893–907, 01 2016.
- [34] E. A. Allen and J. P. Swensen, "Directional stiffness control through geometric patterning and localized heating of fields metal lattice embedded in silicone," *Actuators*, vol. 7, no. 4, p. 80, Nov. 2018.
- [35] R. M. Murray, Z. Li, and S. S. Sastry, A mathematical introduction to robotic manipulation. CRC Press, 1994.